Real-time observation of DNA target interrogation and product release by the RNA-guided endonuclease CRISPR Cpf1 (Cas12a)

Digvijay Singh[a], John Mallon[b], Anustup Poddar[a], Yanbo Wang[a], Ramreddy Tippana[c], Olivia Yang[a], Scott Bailey[a,b], and Taekjip Ha[a,c,d,e,1]

[a]Department of Biophysics and Biophysical Chemistry, Johns Hopkins University School of Medicine, Baltimore, MD 21205; [b]Bloomberg School of Public Health, Johns Hopkins University School of Medicine, Baltimore, MD 21205; [c]Department of Biophysics, Johns Hopkins University, Baltimore, MD 21218; [d]Department of Biomedical Engineering, Johns Hopkins University, Baltimore, MD 21205; and [e]Howard Hughes Medical Institute, Baltimore, MD 21205

Edited by Joseph D. Puglisi, Stanford University School of Medicine, Stanford, CA, and approved April 17, 2018 (received for review October 26, 2017)

CRISPR-Cas9, which imparts adaptive immunity against foreign genomic invaders in certain prokaryotes, has been repurposed for genome-engineering applications. More recently, another RNA-guided CRISPR endonuclease called Cpf1 (also known as Cas12a) was identified and is also being repurposed. Little is known about the kinetics and mechanism of Cpf1 DNA interaction and how sequence mismatches between the DNA target and guide-RNA influence this interaction. We used single-molecule fluorescence analysis and biochemical assays to characterize DNA interrogation, cleavage, and product release by three Cpf1 orthologs. Our Cpf1 data are consistent with the DNA interrogation mechanism proposed for Cas9. They both bind any DNA in search of protospacer-adjacent motif (PAM) sequences, verify the target sequence directionally from the PAM-proximal end, and rapidly reject any targets that lack a PAM or that are poorly matched with the guide-RNA. Unlike Cas9, which requires 9 bp for stable binding and ∼16 bp for cleavage, Cpf1 requires an ∼17-bp sequence match for both stable binding and cleavage. Unlike Cas9, which does not release the DNA cleavage products, Cpf1 rapidly releases the PAM-distal cleavage product, but not the PAM-proximal product. Solution pH, reducing conditions, and 5′ guanine in guide-RNA differentially affected different Cpf1 orthologs. Our findings have important implications on Cpf1-based genome engineering and manipulation applications.

CRISPR | CRISPR-Cpf1 | single molecule | CRISPR-Cas12a | gene editing

In bacteria, clustered regularly interspaced short palindromic repeats, CRISPR-associated (CRISPR-Cas) acts as an adaptive defense system against foreign genetic elements (1). The system achieves adaptive immunity by storing short sequences of invader DNA into the host genome, which get transcribed and processed into small CRISPR RNA (crRNA). These crRNAs form a complex with a CRISPR nuclease to guide the nuclease to complementary foreign nucleic acids (protospacers) for cleavage. Binding and cleavage also require that the protospacer be adjacent to the protospacer adjacent motif (PAM) (2, 3). CRISPR-Cas9, chiefly the Cas9 from *Streptococcus pyogenes* (SpCas9), has been repurposed to create an RNA-programmable endonuclease for gene knockout and editing (4–6). Nuclease-deficient Cas9 has also been used for tagging genomic sites in wide-ranging applications (4–6). This repurposing has revolutionized biology and sparked a search for other CRISPR-Cas enzymes (7, 8). One such search led to the discovery of the Cas protein Cpf1, with some of its orthologs reporting highly specific cleavage activities in mammalian cells (9–12).

Compared with Cas9, Cpf1 has an AT rich PAM (5′-YTTN-3′ vs. 5′-NGG-3′ for SpCas9), a longer protospacer (24 bp vs. 20 bp for Cas9), creates staggered cuts distal to the PAM vs. blunt cuts proximal to the PAM by Cas9 (9) (Fig. 1*A*), and is an even simpler system than Cas9 because it does not require a transactivating RNA for nuclease activity or guide-RNA maturation (13). Off-target effects remain one of the top concerns for CRISPR-based applications, but Cpf1 is reportedly more specific than Cas9 (10, 11). However, its kinetics and mechanism of DNA recognition, rejection, cleavage, and product release as a function of mismatches between the guide-RNA and target DNA remain unknown. Precise characterization of differences among different CRISPR enzymes should help in expanding the functionalities of the CRISPR toolbox.

Here, we used single-molecule fluorescence analysis and biochemical assays to understand how mismatches between the guide-RNA and DNA target modulate the activity of three Cpf1 orthologs from *Acidaminococcus* sp. (AsCpf1), *Lachnospiraceae bacterium* (LbCpf1) and *Francisella novicida* (FnCpf1) (9). Single-molecule methods have been helpful in the study of CRISPR mechanisms (14–23) because they allow real-time detection of reaction intermediates and transient states (24).

Results

Real-Time DNA Interrogation by Cpf1-RNA. We employed a single-molecule fluorescence resonance energy transfer (smFRET) binding assay (25, 26). DNA targets (donor-labeled, 82 bp long) were immobilized on a polyethylene glycol (PEG) passivated surface, and Cpf1 precomplexed with acceptor-labeled guide-RNA (Cpf1-RNA) was added. Cognate DNA and guide-RNA sequences are identical to the Cpf1 ortholog-specific sequences that were previously characterized biochemically (9), with the exception that we used canonical guide-RNA of AsCpf1 for

Significance

Adaptive immunity against foreign DNA elements in microbes, conferred by their CRISPR systems, has been repurposed for wide-ranging genome-engineering applications. The CRISPR-Cas9 system has been the most widely used system. But to overcome some of its major limitations, the search for novel CRISPR enzymes has been a significant area of interest. One such search led to the discovery of CRISPR-Cpf1 systems. We used single-molecule fluorescence analysis and biochemical assays to characterize the kinetics, specificity, and mechanism of Cpf1's DNA interrogation, cleavage, and cleavage-product release. Some major differences from Cas9 were observed which will help the use of Cpf1 in areas outside the realm of Cas9 and effectively broaden the scope of CRISPR-based applications.

Author contributions: D.S. and T.H. designed research; D.S. and J.M. performed research; D.S. and R.T. contributed new reagents/analytic tools; D.S., J.M., A.P., Y.W., O.Y., and S.B. analyzed data; and D.S. and T.H. wrote the paper.

The authors declare no conflict of interest.

This article is a PNAS Direct Submission.

[1]To whom correspondence should be addressed. Email: tjha@jhu.edu.

This article contains supporting information online at www.pnas.org/lookup/suppl/doi:10.1073/pnas.1718686115/-/DCSupplemental.

Published online May 7, 2018.

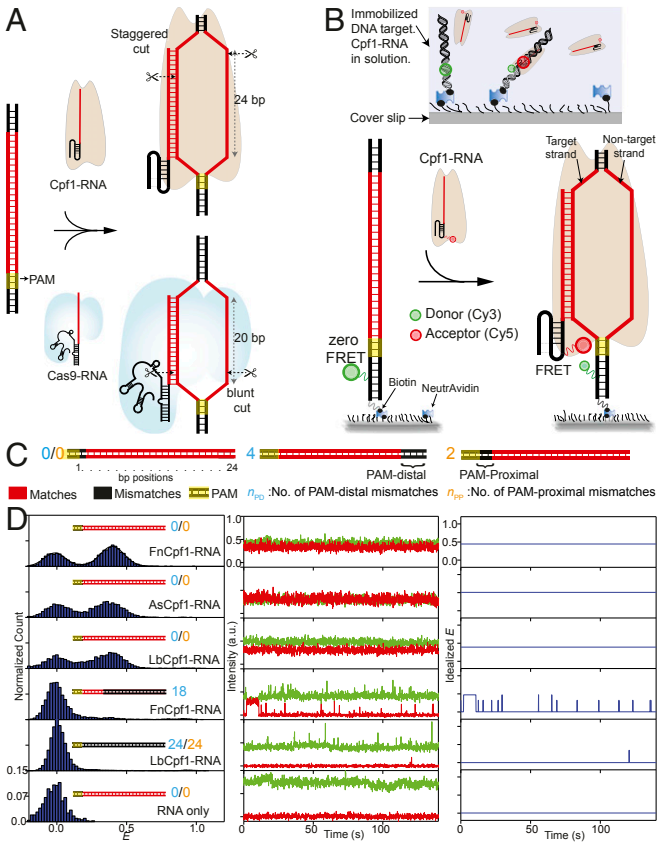

Fig. 1. smFRET assay to study DNA interrogation by Cpf1-RNA. (*A*) Schematic of DNA targeting by CRISPR-Cpf1 and CRISPR-Cas9, and comparison between them. In recent structures (27, 30, 32), the last four PAM-distal base pairs were not unwound and without any RNA-DNA base-pairing for some orthologs. It is unknown whether this is a common feature of all Cpf1 enzymes, and, currently, the protospacer for Cpf1 is still taken to be 24 bp long. (*B*) Schematic of a single-molecule FRET assay. Cy3-labeled DNA immobilized on a passivated surface is targeted by a Cy5-labeled guide-RNA in complex with Cpf1, referred to as Cpf1-RNA. (*C*) DNA targets with mismatches in the protospacer region against the guide-RNA. The number of mismatches PAM-distal (n_{PD}) and PAM-proximal (n_{PP}) are shown in cyan and orange, respectively. (*D*) *E* histograms (*Left*) at 50 nM Cpf1-RNA or 50 nM RNA only. Representative single-molecule intensity time traces of donor (green) and acceptor (red) are shown (*Center*), along with *E* values idealized (*Right*) by hidden Markov modeling (29).

FnCpf1 analysis because guide-RNAs of AsCpf1 and FnCpf1 are interchangeable (9) (*SI Appendix*, Fig. S1). Locations of donor (Cy3) and acceptor (Cy5) fluorophores were chosen such that FRET would report on interaction between the DNA target and Cpf1-RNA (27) (Fig. 1*B* and *SI Appendix*, Fig. S1). Fluorescent labeling did not affect cleavage activity of Cpf1-RNA (*SI Appendix*, Fig. S2). We used a series of DNA targets containing different degrees of mismatches relative to the guide-RNA referred to here with n_{PD} (the number of PAM-distal mismatches) or n_{PP} (the number of PAM-proximal mismatches) (Fig. 1*C*).

The cognate DNA target in the presence of 50 nM Cpf1-RNA gave two distinct populations, with FRET efficiency *E* centered at 0.4 and 0. Using instead a noncognate DNA target (n_{PD} of 24 and without PAM) or guide-RNA only without Cpf1 gave a negligible $E = 0.4$ population, allowing us to assign $E \approx 0.4$ to a sequence-specific Cpf1–RNA–DNA complex where the labeling sites are separated by 54 Å (27) (Fig. 1*D* and *SI Appendix*, Fig. S1). The $E = 0$ population is a combination of unbound states and bound states with an inactive or missing acceptor. smFRET time trajectories of the cognate DNA target showed a constant $E \approx 0.4$ value within measurement noise (Fig. 1*D*).

Cpf1-RNA titration experiments yielded dissociation constants (K_d) of 0.27 nM (FnCpf1), 0.1 nM (AsCpf1), and 3.9 nM (LbCpf1) in our standard imaging condition and 0.13 nM (LbCpf1) in a reducing condition (*SI Appendix*, Fig. S3). Binding is much tighter than the 50 nM K_d previously reported for FnCpf1 (13). We performed purification and biochemical experiments in buffer containing DTT as per previous protocols (9) but did not include DTT for standard imaging conditions because of severe fluorescence intermittency of Cy5 caused by DTT (28). DTT did not affect FnCpf1 or AsCpf1 DNA binding but made binding >20-fold tighter for LbCpf1 (*SI Appendix*, Fig. S3). Cleavage by AsCpf1 is most effective at pH 6.5 to 7.0 (*SI Appendix*, Fig. S4). Therefore, we used pH 7.0 for AsCpf1 and standard pH 8.0 for FnCpf1 and LbCpf1.

E histograms obtained at 50 nM Cpf1-RNA show the impact of mismatches on DNA binding (Fig. 2). The apparent bound fraction f_{bound}, defined as the fraction of DNA molecules with $E > 0.2$, remained unchanged when n_{PD} increased from 0 to 7 (0 to 6 for LbCpf1 in nonreducing conditions) (Figs. 2 and 3*G*). Binding was ultrastable for $n_{PD} \leq 7$; f_{bound} did not change even 1 h after washing away free Cpf1-RNA (Fig. 3*A*). f_{bound} decreased steeply when n_{PD} exceeded 7 for FnCpf1 and LbCpf1, but the decrease was gradual for AsCpf1 and for LbCpf1 in the reducing condition (Figs. 2 and 3*G*). For all Cpf1 orthologs, ultrastable binding required $n_{PD} \leq 7$, corresponding to a 17-bp PAM-proximal sequence match. This is much larger than the 9-bp PAM-proximal sequence match required for ultrastable binding of Cas9 (19). PAM-proximal mismatches are highly deleterious for

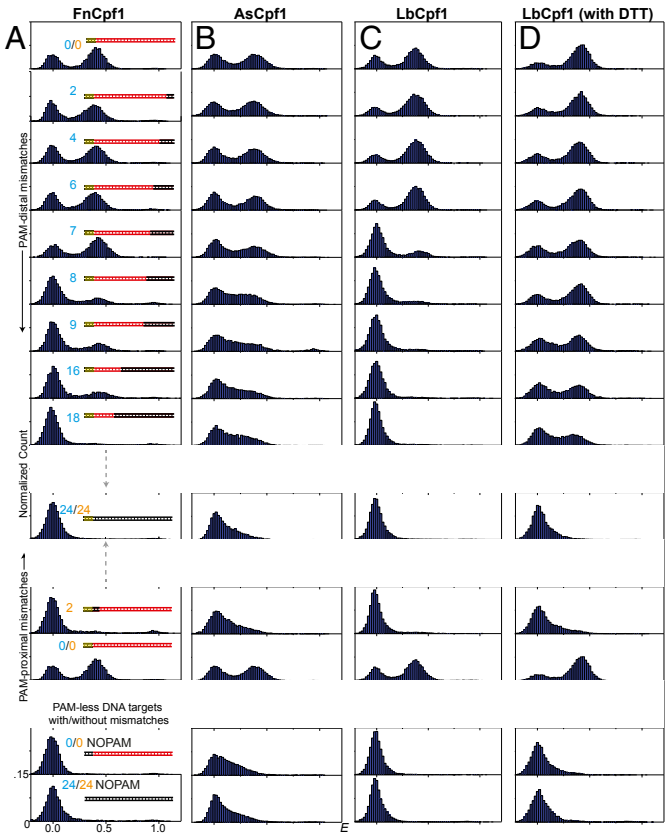

Fig. 2. *E* histograms during DNA interrogation by Cpf1-RNA. (*A*) FnCpf1. (*B*) AsCpf1. (*C*) LbCpf1. (*D*) LbCpf1 (in reducing conditions of 5 mM DTT). The number of PAM-distal (n_{PD}) and PAM-proximal mismatches (n_{PP}) is shown in cyan and orange respectively. [Cpf1-RNA] = 50 nM. The third peak at high FRET efficiencies occurred in only some experiments and was the result of fluorescent impurities likely due to variations in PEG passivation, and they were difficult to exclude in automated analysis.

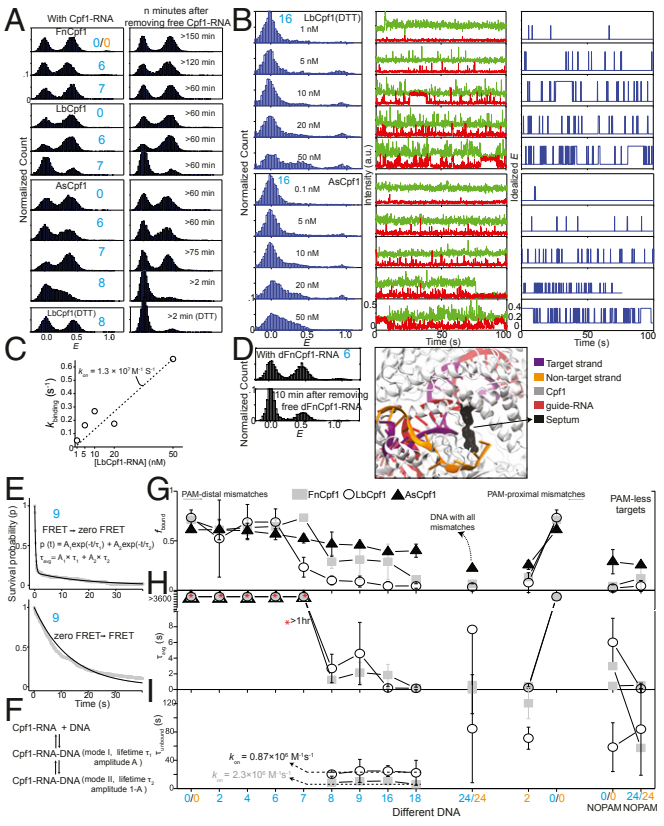

Fig. 3. Dynamic interaction of Cpf1-RNA with DNA as a function of mismatches. (*A*) *E* histograms for various n_{PD} with 50 nM Cpf1-RNA (*Left*) and indicated minutes after free Cpf1-RNA was washed out (*Right*) for FnCpf1, LbCpf1, AsCpf1, and LbCpf1 in reducing condition of 5 mM DTT. (*B*) *E* histograms (*Left*) and representative smFRET time trajectories (*Center*) with their idealized *E* values (*Right*) for n_{PD} = 16 at various concentrations of LbCpf1-RNA in reducing condition and AsCpf1-RNA. The third peak at high FRET efficiencies occurred in only some experiments and was the result of fluorescent impurities likely due to variations in PEG passivation, and they were difficult to exclude in automated analysis. (*C*) Rate of LbCpf1-RNA and DNA association ($k_{binding}$) at different LbCpf1-RNA concentration. $E > 0.2$ and $E < 0.2$ states were taken as putative bound and unbound states. Dwell times of the unbound states were used to calculate $k_{binding}$. (*D*) Compared with FnCpf1, dFnCpf1 dissociates much quicker from DNA as shown by the change in bound population with and after removal of free dFnCpf1-RNA (*Left*). A septum, preventing the rehybridization of target and nontarget strand, emerges after DNA cleavage which could prevent dissociation of Cpf1-RNA as shown in the structure of FnCpf1-RNA-DNA postcleavage (*Right*) (PDB ID code 5MGA) (30). (*E*) Survival probability of FRET state ($E > 0.2$; putative bound states) and zero FRET state ($E < 0.2$; unbound states) dwell times vs. time, fit with double-exponential and single-exponential decay to obtain lifetime of bound state (τ_{avg}) and unbound state ($\tau_{unbound}$), respectively. (*F*) A Model describing a bimodal binding nature of Cpf1-RNA. (*G*) f_{bound}, (*H*) bound state lifetime, and (*I*) unbound state lifetime for various mismatches at 50 nM Cpf1-RNA. The average of rates of binding ($\tau_{unbound}^{-1}$) of DNA with n_{PD} = 8–18 were used to calculate k_{on} for FnCpf1 and LbCpf1. n_{PD} and n_{PP} are shown in cyan and orange, respectively.

Cpf1 binding because f_{bound} dropped by more than 95% if $n_{PP} \geq 2$ (Figs. 2 and 3*G*). In comparison, Cas9 showed a more modest ~50% drop for $n_{PP} = 2$ (19). Overall, Cpf1 is much better than Cas9 in discriminating against both PAM-distal and PAM-proximal mismatches for stable binding.

Single-molecule time trajectories of all Cpf1 orthologs for $n_{PD} \leq 7$ showed a constant $E \approx 0.4$ value within noise, limited only by photobleaching. For $n_{PD} > 7$, we observed reversible transitions in *E* likely due to transient binding (*SI Appendix*, Figs. S5–S7). Dwell time analysis as a function of Cpf1-RNA concentration confirmed that *E* fluctuations are due to binding and dissociation, not conformational changes (Fig. 3 *B* and *C* and *SI Appendix*, Fig. S3). We used hidden Markov modeling analysis (29) to segment the time traces to bound and unbound states. Average lifetime of the bound state, τ_{avg}, was >1 h for $n_{PD} \leq 7$ but decreased to a few seconds with $n_{PD} > 7$ or any PAM-proximal mismatches (Fig. 3*H*). The unbound state lifetime differed between orthologs but was nearly the same among most DNA targets, indicating that initial binding has little sequence dependence. The bimolecular association rate k_{on} was 2.37×10^6 $M^{-1}{\cdot}s^{-1}$ (FnCpf1), 0.87×10^6 $M^{-1}{\cdot}s^{-1}$ (LbCpf1), and 1.33×10^7 $M^{-1}{\cdot}s^{-1}$ (LbCpf1 in reducing conditions) (Fig. 3 *C* and *I*). Much longer apparent unbound state lifetimes with PAM-proximal mismatches or DNA targets without PAM are likely due to binding events shorter than the time resolution (0.1 s).

These results indicate that Cpf1-RNA has dual binding modes. It first binds DNA nonspecifically (mode I) in search of PAM, and, upon detection of PAM, RNA-DNA heteroduplex formation ensues (mode II), and, if it extends ≥17 bp, Cpf1-RNA remains ultrastably bound to the DNA (Fig. 3*F* and *SI Appendix*, Fig. S8). Some reversible transitions in *E* were observed for DNA with $n_{PD} = 7$, indicating that multiple short-lived binding events take place before DNA is cleaved and transitioning to ultrastable binding (*SI Appendix*, Figs. S5–S7 and S13). RNA-DNA heteroduplex extension is likely directional from the PAM-proximal to PAM-distal end because any PAM-proximal mismatch prevented stable binding. Consistent with dual binding modes, survival probability distributions of bound and unbound state were best described by a double and single exponential decay, respectively (Fig. 3*E*).

DNA Cleavage by Cpf1 as a Function of Mismatches. Next, we performed gel-based experiments using the same set of DNA targets to measure cleavage by Cpf1. Cleavage was observed at a wide range of temperatures (4 to 37 °C), required divalent ions (Ca^{2+} could substitute for Mg^{2+}), and showed a pH dependence. AsCpf1 is highly active only at slightly acidic to neutral pH (6.5 to 7.0) whereas FnCpf1 has more activity at pH 8.5 than pH 8.0 (*SI Appendix*, Figs. S9–S11). Cleavage required 17 PAM-proximal matches, corresponding to $n_{PD} \leq 7$, (Fig. 4*A* and *SI Appendix*, Figs. S9 and S10), which is identical to the threshold for stable binding (Figs. 2 and 3). This contrasts with Cas9, which requires only 9 PAM-proximal matches for stable binding (19) but 16 PAM-proximal matches for cleavage (3, 14).

We measured the time it takes to cleave DNA, $\tau_{cleavage}$ (*SI Appendix*, Fig. S12). $\tau_{cleavage}$ remained approximately the same among DNA with $0 \leq n_{PD} \leq 6$ for FnCpf1 (30 to 60 s) but steeply increased upon increasing n_{PD} to 7 (Fig. 4 *B* and *C*). AsCpf1 showed a more complex n_{PD} dependence, with a minimal $\tau_{cleavage}$ value of 8 min for $n_{PD} = 6$ (Fig. 4*C*). $\tau_{cleavage}$ is much longer than the 1 to 15 s it takes for Cpf1-RNA to bind the DNA at the same Cpf1-RNA concentration, suggesting that Cpf1–RNA–DNA undergoes additional rate-limiting steps after DNA binding and before cleavage. These additional steps are likely the conformational rearrangement of the Cpf1–RNA–DNA complex that positions the nuclease domains and DNA strands for cleavage, as has been described in structural analysis of the Cpf1–RNA–DNA complex (27, 30).

Because $\tau_{cleavage}$ is shorter than 60 s for FnCpf1 on DNA targets with $n_{PD} < 7$, we can infer that the ultrastable binding observed for FnCpf1 on the same DNA (lifetime > 1 h) is to the cleaved product. Therefore, it is in principle possible that cleavage stabilizes Cpf1-RNA binding and that, before cleavage, Cpf1-RNA binds to the target DNA less stably. To test this possibility, we purified catalytically dead FnCpf1 (dFnCpf1; D917A mutation) (9) and performed the DNA interrogation experiment. dFnCpf1 binding was ultrastable for cognate DNA but showed a substantial dissociation after 5 to 10 min for n_{PD} = 6 or 7 (Fig. 3*D* and *SI Appendix*, Fig. S13). Therefore, cleavage can further stabilize Cpf1-RNA binding to DNA. A septum separating the target and nontarget strands and preventing their rehybridization was observed only after cleavage in Cpf1–RNA–DNA structure (27, 30–32). The formation of this septum during/after

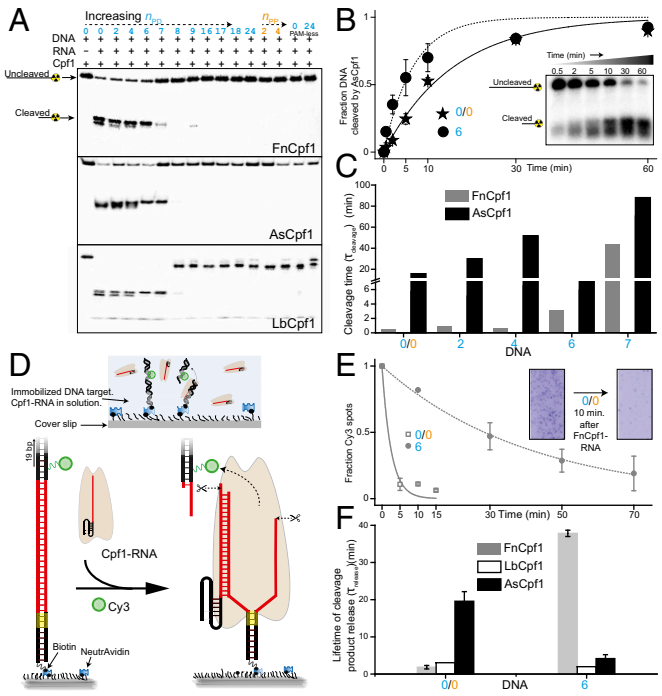

Fig. 4. DNA cleavage and product release. (*A*) Cpf1 induced DNA cleavage at room temperature analyzed by 10% denaturing polyacrylamide gel electrophoresis of radio-labeled DNA targets. (*B*) Fraction of DNA cleaved by AsCpf1 vs. time for cognate and DNA with n_{PD} = 6, and single-exponential fits. A representative gel image is shown in the *Inset*. (*C*) Cleavage time ($\tau_{cleavage}$) determined from cleavage time courses as shown in *B*. (*D*) Schematic of single-molecule cleavage product release assay. PAM-distal cleavage product release can be detected as the disappearance of the fluorescence signal from Cy3 attached to the PAM-distal product. (*E*) Average fraction of Cy3 spots remaining vs. time for FnCpf1-RNA (50 nM). The *Inset* shows images before and after 10-min reaction. (*F*) Average time of cleavage product release ($\tau_{release}$).

DNA cleavage could be the basis of higher stability of Cpf1-RNA binding to DNA postcleavage. Cleavage was negligible for DNA targets that showed transient binding. Therefore, transient binding and dissociation we observed does not result from a cleaved DNA product.

Fate of Cleaved DNA. For the downstream processing of a cleaved DNA, the cleaved site needs to be exposed (33). To investigate the fate of the target DNA after cleavage, we relocated the Cy3 label to the PAM-distal DNA segment that would depart the imaging surface if the Cpf1 releases the cleavage product(s) (Fig. 4*D* and *SI Appendix*, Fig. S14). The number of fluorescent spots decreased over time (Fig. 4*E*), suggesting that the cleavage product is released under physiological conditions, which is in stark contrast to Cas9, which holds onto the cleaved DNA and does not release except in denaturing condition (14, 19). Cpf1 releases only the PAM-distal cleavage product, however, because, when Cy3 is attached to a site on the PAM-proximal cleavage product, the number of fluorescence spots did not decrease over time (Figs. 1–3). The average time for fluorescence signal disappearance ranged from ∼30 s to 30 min, depending on the PAM-distal mismatches and Cpf1 orthologs. By subtracting the time it takes to bind and cleave, we estimated the product release time scale ($\tau_{release}$) (Fig. 4*F*), which showed a dependence on n_{PD}. Therefore, PAM-distal mismatches can also affect product release.

Discussion

The two-step mechanism of sampling for PAM followed by directional RNA-DNA heteroduplex extension (Fig. 5) is shared between Cas9 and Cpf1, suggesting this to be a general target identification mechanism of these CRISPR systems. Ultrastable binding of Cpf1 requires the same extent of sequence match (17-bp PAM-proximal matches) as target cleavage. This contrasts with Cas9, which requires only 9 bp and 16 bp PAM-proximal matches for ultrastable binding and cleavage, respectively (19, 34, 35). Therefore, Cpf1 can be more sequence-specific in experiments involving the use of catalytically dead CRISPR enzymes for imaging, tracking, and transcription regulation purposes (36). The binding specificity of engineered Cas9s [eCas9 (37) and Cas9-HF1 (38)] is still much lower than that of Cpf1 (35). Therefore, Cpf1 has the potential to be a better alternative to all current Cas9 variants.

Cleavage rate is reduced with increasing PAM-distal mismatches (Fig. 4*C*) even when the mismatches do not affect stable binding (Fig. 3), suggesting that shorter RNA-DNA heteroduplexes result in slower conformational changes required for cleavage activation. Previous studies on Cas9 revealed that mismatches alter the kinetics of DNA unwinding, RNA-DNA heteroduplex extension, and nuclease and proof-reading domain movements (20, 22, 34, 35).

For cognate DNA target, RNA-DNA heteroduplex extension would require unwinding of the parental DNA duplex. We performed cleavage experiments using DNA with the PAM-distal mismatched region preunwound to test the relative importance of parental DNA duplex unwinding and annealing with RNA in cleavage activation. Cpf1 needed many fewer PAM-proximal matches to cleave if the mismatched region was preunwound (*SI Appendix*, Fig. S15), indicating indeed that DNA unwinding is likely more important than RNA-DNA heteroduplex in activating cleavage. Accordingly, ssDNA can also be cleaved by Cpf1 (*SI Appendix*, Fig. S15). Therefore, the role of RNA may primarily be in keeping the DNA unwound through annealing with the target strand.

CRISPR enzymes bend DNA to cause a local kink near the PAM, which acts as a seed for unwinding and heteroduplex extension (27, 39, 40). Perturbing DNA rigidity by introducing a nick near the PAM slowed down cleavage, underscoring the importance of Cpf1-induced DNA bending for cleavage (*SI Appendix*, Fig. S16). Cas9 causes a larger DNA bend than Cpf1 (27, 39), possibly contributing to its higher tolerance of PAM-proximal mismatches in binding and cleavage activity.

Shorter and simpler guide-RNA (9) for Cpf1 could potentially be deleterious for its engineering or extension, as is done for Cas9's guide-RNA (41). For example, an extra 5′ guanine in the guide-RNA was extremely deleterious for cleavage by LbCpf1 (*SI Appendix*, Fig. S17), potentially posing problems for applications where guide-RNAs are transcribed using U6/T7 RNA polymerase systems that require the first nucleotide in transcribed RNA to be the guanine (42, 43). This problem may be solved by transcribing RNAs with 5′ G containing CRISPR repeat which will be processed out by Cpf1 itself to produce mature guide-RNAs (13) (*SI Appendix*, Fig. S17).

Cas9 has provided a highly efficient and versatile platform for DNA targeting, but the efficiency of gene knock-in is low (44). Among the possible reasons is the inability of Cas9 to release and expose cleaved DNA ends. In contrast, the ability of Cpf1 to release a cleavage product readily, combined with the staggered cuts it generates, could in principle increase the knock-in efficiency. Although it remains to be seen how this property affects the downstream processing in vivo, we can also envision a scenario where product release by Cpf1 can be detrimental to genome engineering applications. Applying positive twist to the DNA in a Cas9–RNA–DNA complex can release Cas9-RNA from DNA by promoting rewinding of the parental DNA duplex (15). Positive supercoiling is generated ahead of a transcribing RNA polymerase (45), and Cas9 holding onto the double strand break product may help build the torsional strain required to eject Cas9-RNA. If the PAM-distal cleavage product is released prematurely, as in the case of Cpf1, transcription-induced positive supercoiling cannot build up, and the Cpf1-RNA would

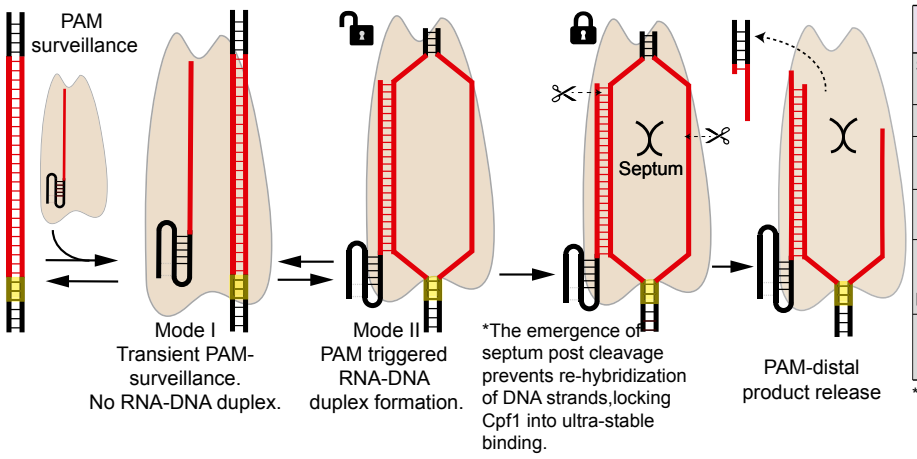

Parameter	FnCpf1	AsCpf1	LbCpf1	SpCas9
Stable binding specifity	17 bp*	17 bp*	17 bp*	9 bp*
k_{on}	Slow	Ultra fast	Ultra fast	#
Cleavage specificity	17 bp*	17 bp*	17 bp*	16 bp*
Rate of Cleavage	Slightly Slow	Ultra Slow		#
Rate of cleavage product release	Fast	Slow	Ultra-fast	zero (#)
Effect of pH & reducing conditions	Marginal	Substantial	Substantial	

* PAM-proximal matches # Point of Reference

Fig. 5. Model of Cpf1-RNA DNA targeting, cleavage, and product release.

remain bound stably to the PAM-proximal cleavage product, hiding the cleaved end and preventing efficient knock-in.

High specificity of adaptive immunity by Cpf1 against hypervariable genetic invaders is a little paradoxical. But Cpf1 and Cas9 systems coexist in many species, and thus they likely provide immunity suited to their features, effectively broadening the scope of immunity. Overall, our results establish major different and common features between Cpf1 and Cas9 which can be useful for the broadening of genome engineering applications as well.

Materials and Methods

DNA Targets for smFRET Analysis of DNA Interrogation. Single-stranded DNA (ssDNA) oligonucleotides were purchased from Integrated DNA Technologies. ssDNA target and nontarget (labeled with Cy3) strands and a biotinylated adaptor strand were mixed. The nontarget strand was created by ligating two component strands, one with Cy3 and the other containing the protospacer region to avoid having to synthesize modified oligos for each mismatch construct. For schematics, see *SI Appendix*, Fig. S1*A*. Fully duplexed DNA targets but with a nick were also used. The Cy3 fluorophore is located 4 bp upstream of the protospacer adjacent motif (PAM: 5′-YTTN-3′) and was conjugated via Cy3 *N*-hydroxysuccinimido (Cy3-NHS; GE Healthcare) to the Cy3 oligo at amino-group attached to a modified thymine through a C6 linker (amino-dT) using NHS ester linkage. smFRET experiments were done with both sets of DNA targets (with or without a nick), and no significant differences were found between them. *SI Appendix*, Table S1 shows all DNA targets used. Additional details about the DNA targets are available in *SI Appendix*,*Additional Details About Materials and Methods*.

DNA Targets for Real-Time Single-Molecule Assay for Interrogating Fate of Cleaved DNA. For single-molecule cleavage product release experiments, a nontarget strand with the Cy3 relocated in a different position was used. A Cy3 label was conjugated onto the amine modification (amino-dT) using Cy3-NHS, as described above. A schematic of these DNA targets is in *SI Appendix*, Fig. S14, and their sequences are in *SI Appendix*, Table S5.

DNA Targets for Gel Electrophoresis Experiments. DNA targets were prepared and hybridized as described above. For radio-labeled gel electrophoresis experiments, the target strand was 5′ radiolabeled with T4 polynucleotide kinase (New England BioLabs) and γ-^{32}P ATP (Perkin-Elmer). The target and nontarget strands were annealed with the nontarget strands in excess.

Guide-RNA. For single-molecule experiments, guide-RNA was purchased from IDT with modifications for Cy5 labeling as described in *SI Appendix*, Table S5. Cy5 was conjugated via Cy5 *N*-hydroxysuccinimido (Cy5-NHS; GE Healthcare) to the RNA as described previously (19, 46). For all other experiments, unmodified guide-RNA was used, and they were either in vitro transcribed or purchased from IDT. Guide-RNA sequences used in this study are available in *SI Appendix*, Table S5.

Preparation of Cpf1-RNA. The Cpf1-RNA was freshly prepared before each experiment by mixing the guide-RNA (50 nM) and Cpf1 in a 1:3.5 ratio in the following reaction buffers and incubated for at least 10 min at room temperature: for FnCpf1 and LbCpf1, 50 mM Tris·HCl (pH 8.0), 100 mM NaCl, and 10 mM $MgCl_2$; for AsCpf1, 50 mM Hepes (pH 7.0), 100 mM NaCl, and 10 mM $MgCl_2$ (5 mM DTT was only used in the buffer when specified). For single-molecule fluorescence experiments, 0.2 mg/mL BSA, 1 mg/mL glucose oxidase, 0.04 mg/mL catalase, 0.8% dextrose, and saturated Trolox (>5 mM) were additional contents of the reaction buffers. Excess Cpf1 was used to achieve the highest extent of complexation of all of the available guide-RNA, and the concentration of guide-RNA was used as the concentration of Cpf1-RNA. Cpf1 activity using the similar guide-RNA and on DNA targets with the same protospacer and PAM has been characterized previously (9). Fluorophore labeling of either DNA targets or guide-RNA did not impair Cpf1 activity (*SI Appendix*, Fig. S2).

Expression-Purification of Cpf1 and Single-Molecule Detection. Methods have been described previously (9, 26). Their full details are available in *SI Appendix*,*Additional Details About Materials and Methods*.

FRET Efficiency Histograms and Cpf1-RNA Bound DNA Fraction. An smFRET time trajectory is a series of E values every 100 ms. The first five E values of each single-molecule trace were pooled together to build single-molecule E histograms. The Cpf1-RNA bound DNA fraction (f_{bound}) was calculated as a ratio between the number of molecules with $E > 0.2$ and the total number of molecules in the E histograms. E histograms shown in Fig. 2 were constructed by combining data from two independent experiments (except for AsCpf1; PAM-less DNA). At least 2,000 molecules, in most cases >4,000, were used for each histogram. The criteria for the selection of the fluorescent single-molecule spot was the same as described previously. A majority of selected spots (~85%) were used for analysis. The remaining (~15%) were discarded as their intensities were too low (likely due to impurities) or too high (impurities, aggregates, or multiple fluorescent molecules in a single spot).

Determination of Binding Kinetics. For DNA targets that showed real-time reversible binding/dissociation of Cpf1-RNA, idealization of smFRET traces via hidden Markov model (29) analysis yielded two predominant FRET states, of zero ($E < 0.2$) and bound state ($E > 0.2$). The lifetime of the unbound state, $\tau_{unbound}$, was calculated by fitting the survival probability of dwell times of the unwound state ($E < 0.2$) vs. time to a single-exponential decay ($\exp[-t/\tau_{unbound}]$). The survival probability of the bound state required a double-exponential decay for adequate fitting ($A * \exp[-t/\tau_1] + [1 - A] * \exp[-t/\tau_2]$), and the average lifetime was calculated as $\tau_{avg} = A\tau_1 + (1 - A)\tau_2$. At least 60 long-lived smFRET traces, in most cases >90, were used for the indicated lifetime analysis(es). The bimolecular association rate constant k_{on}, binding rate $k_{binding}$, and dissociation rate k_{off} were calculated as follows:

$$k_{binding} = \tau_{unbound}^{-1}$$

$$k_{off} = \tau_{bound}^{-1}$$

$$k_{on} = k_{binding}/[\text{Cpf1-RNA}].$$

Due to under-sampled binding events, τ_{avg} of FnCpf1 for PAM-less DNA and

DNA with 2 n_{PP} were calculated as the algebraic average of $E > 0.2$ dwell times. Cy5 labeling efficiency of guide-RNA was ~90%, and thus f_{bound} and $\tau_{unbound}$ were appropriately corrected. Due to high noise, the smFRET traces from experiments involving AsCpf1 could not be idealized with high accuracy, thus preventing their k_{off} and k_{on} analysis.

Estimation of Dissociation Constant (K_d). To estimate K_d, Cpf1-RNA bound DNA fraction (f_{bound}) vs. Cpf1-RNA concentration (c) was fit using $f_{bound} = M \times c/(K_d + c)$ where M is the maximum observable f_{bound}. M is typically less than 1 because of inactive or missing acceptors or because not all of the DNA on the surface are capable of binding Cpf1-RNA.

Overall Lifetime of Release of Cleavage Products. Single-molecule experiments were used to estimate the lifetime of the release of cleavage products by fitting the decreasing number of Cy3 spots (loss of spots due to Cpf1-RNA–induced cleavage and release) to a single-exponential decay. The time of binding ($k_{on} \times 50$ nM) and time of cleavage ($\tau_{cleavage}$) were subtracted from the obtained lifetime to get the true lifetime of the release ($\tau_{release}$) of cleavage products. But, since $\tau_{cleavage}$ was not measured for LbCpf1, its reported $\tau_{release}$ is without the $\tau_{cleavage}$ and time of binding subtraction.

Gel Electrophoresis Experiments and Autoradiography. Experiments containing radiolabeled DNA substrates were performed as above. However, samples were quenched in buffer containing 95% formamide, 0.01% SDS, 0.01% bromophenol blue, 0.01% xylene cyanol, and 1 mM EDTA and incubated at 95 °C for 5 min, and then on ice for 2 min. The volume ratio of quenching buffer to reaction was 5:1. Samples were loaded onto denaturing polyacrylamide gels [10% acrylamide, 50% (wt/vol) urea] and allowed to separate. The amount of sample loaded onto gel was normalized to 10,000 counts per sample. Gels were imaged via phosphor screens. The entire panel of DNA targets used in these gel-electrophoresis experiments is available in *SI Appendix*, Table S2. All of the gel electrophoresis experiments were done in the following reaction buffers: for FnCpf1 and LbCpf1, 50 mM Tris·HCl (pH 8.0), 100 mM NaCl, 10 mM $MgCl_2$, and 5 mM DTT; for AsCpf1, 50 mM Hepes (pH 7.0), 100 mM NaCl, 10 mM $MgCl_2$, and 5 mM DTT. For all experiments (single-molecule fluorescence analysis and gel electrophoresis experiments), errors bars represent SD from the analysis of two or three replicate experiments.

ACKNOWLEDGMENTS. The project was supported by National Science Foundation Grant PHY-1430124 (to T.H.) and National Institutes of Health Grants GM065367 and GM112659 (to T.H.) and GM097330 (to S.B.). T.H. is an investigator with the Howard Hughes Medical Institute. J.M. is supported by National Institutes of Health Chemistry–Biology Interface Training Program Grant T32GM080189.

1. Marraffini LA, Sontheimer EJ (2010) CRISPR interference: RNA-directed adaptive immunity in bacteria and archaea. *Nat Rev Genet* 11:181–190.
2. Gasiunas G, Barrangou R, Horvath P, Siksnys V (2012) Cas9-crRNA ribonucleoprotein complex mediates specific DNA cleavage for adaptive immunity in bacteria. *Proc Natl Acad Sci USA* 109:E2579–E2586.
3. Jinek M, et al. (2012) A programmable dual-RNA-guided DNA endonuclease in adaptive bacterial immunity. *Science* 337:816–821.
4. Barrangou R, Doudna JA (2016) Applications of CRISPR technologies in research and beyond. *Nat Biotechnol* 34:933–941.
5. Wang H, La Russa M, Qi LS (2016) CRISPR/Cas9 in genome editing and beyond. *Annu Rev Biochem* 85:227–264.
6. Wright AV, Nuñez JK, Doudna JA (2016) Biology and applications of CRISPR systems: Harnessing nature's toolbox for genome engineering. *Cell* 164:29–44.
7. Shmakov S, et al. (2017) Diversity and evolution of class 2 CRISPR-Cas systems. *Nat Rev Microbiol* 15:169–182.
8. Burstein D, et al. (2017) New CRISPR-Cas systems from uncultivated microbes. *Nature* 542:237–241.
9. Zetsche B, et al. (2015) Cpf1 is a single RNA-guided endonuclease of a class 2 CRISPR-Cas system. *Cell* 163:759–771.
10. Kleinstiver BP, et al. (2016) Genome-wide specificities of CRISPR-Cas Cpf1 nucleases in human cells. *Nat Biotechnol* 34:869–874.
11. Kim D, et al. (2016) Genome-wide analysis reveals specificities of Cpf1 endonucleases in human cells. *Nat Biotechnol* 34:863–868.
12. Makarova KS, et al. (2015) An updated evolutionary classification of CRISPR-Cas systems. *Nat Rev Microbiol* 13:722–736.
13. Fonfara I, Richter H, Bratovič M, Le Rhun A, Charpentier E (2016) The CRISPR-associated DNA-cleaving enzyme Cpf1 also processes precursor CRISPR RNA. *Nature* 532:517–521.
14. Sternberg SH, Redding S, Jinek M, Greene EC, Doudna JA (2014) DNA interrogation by the CRISPR RNA-guided endonuclease Cas9. *Nature* 507:62–67.
15. Szczelkun MD, et al. (2014) Direct observation of R-loop formation by single RNA-guided Cas9 and Cascade effector complexes. *Proc Natl Acad Sci USA* 111:9798–9803.
16. Redding S, et al. (2015) Surveillance and processing of foreign DNA by the Escherichia coli CRISPR-Cas system. *Cell* 163:854–865.
17. Rutkauskas M, et al. (2015) Directional R-loop formation by the CRISPR-Cas surveillance complex cascade provides efficient off-target site rejection. *Cell Rep* 10:1534–1543.
18. Josephs EA, et al. (2016) Structure and specificity of the RNA-guided endonuclease Cas9 during DNA interrogation, target binding and cleavage. *Nucleic Acids Res* 44:2474.
19. Singh D, Sternberg SH, Fei J, Doudna JA, Ha T (2016) Real-time observation of DNA recognition and rejection by the RNA-guided endonuclease Cas9. *Nat Commun* 7:12778.
20. Lim Y, et al. (2016) Structural roles of guide RNAs in the nuclease activity of Cas9 endonuclease. *Nat Commun* 7:13350.
21. Blosser TR, et al. (2015) Two distinct DNA binding modes guide dual roles of a CRISPR-Cas protein complex. *Mol Cell* 58:60–70.
22. Dagdas YS, Chen JS, Sternberg SH, Doudna JA, Yildiz A (2017) A conformational checkpoint between DNA binding and cleavage by CRISPR-Cas9. *Sci Adv* 3:eaao0027.
23. Chen JS, et al. (2017) Enhanced proofreading governs CRISPR-Cas9 targeting accuracy. *Nature* 550:407–410.
24. Joo C, Balci H, Ishitsuka Y, Buranachai C, Ha T (2008) Advances in single-molecule fluorescence methods for molecular biology. *Annu Rev Biochem* 77:51–76.
25. Ha T, et al. (1996) Probing the interaction between two single molecules: Fluorescence resonance energy transfer between a single donor and a single acceptor. *Proc Natl Acad Sci USA* 93:6264–6268.
26. Roy R, Hohng S, Ha T (2008) A practical guide to single-molecule FRET. *Nat Methods* 5:507–516.
27. Yamano T, et al. (2016) Crystal structure of Cpf1 in complex with guide RNA and target DNA. *Cell* 165:949–962.
28. Bates M, Blosser TR, Zhuang X (2005) Short-range spectroscopic ruler based on a single-molecule optical switch. *Phys Rev Lett* 94:108101.
29. McKinney SA, Joo C, Ha T (2006) Analysis of single-molecule FRET trajectories using hidden Markov modeling. *Biophys J* 91:1941–1951.
30. Stella S, Alcón P, Montoya G (2017) Structure of the Cpf1 endonuclease R-loop complex after target DNA cleavage. *Nature* 546:559–563.
31. Stella S, Alcón P, Montoya G (2017) Class 2 CRISPR-Cas RNA-guided endonucleases: Swiss Army knives of genome editing. *Nat Struct Mol Biol* 24:882–892.
32. Swarts DC, van der Oost J, Jinek M (2017) Structural basis for guide RNA processing and seed-dependent DNA targeting by CRISPR-Cas12a. *Mol Cell* 66:221–233.e4.
33. Richardson CD, Ray GJ, DeWitt MA, Curie GL, Corn JE (2016) Enhancing homology-directed genome editing by catalytically active and inactive CRISPR-Cas9 using asymmetric donor DNA. *Nat Biotechnol* 34:339–344.
34. Sternberg SH, LaFrance B, Kaplan M, Doudna JA (2015) Conformational control of DNA target cleavage by CRISPR-Cas9. *Nature* 527:110–113.
35. Singh D, et al. (2018) Mechanisms of improved specificity of engineered Cas9s revealed by single-molecule FRET analysis. *Nat Struct Mol Biol* 25:347–354.
36. Doudna JA, Charpentier E (2014) Genome editing. The new frontier of genome engineering with CRISPR-Cas9. *Science* 346:1258096.
37. Slaymaker IM, et al. (2016) Rationally engineered Cas9 nucleases with improved specificity. *Science* 351:84–88.
38. Kleinstiver BP, et al. (2016) High-fidelity CRISPR-Cas9 nucleases with no detectable genome-wide off-target effects. *Nature* 529:490–495.
39. Jiang F, et al. (2016) Structures of a CRISPR-Cas9 R-loop complex primed for DNA cleavage. *Science* 351:867–871.
40. Anders C, Niewoehner O, Duerst A, Jinek M (2014) Structural basis of PAM-dependent target DNA recognition by the Cas9 endonuclease. *Nature* 513:569–573.
41. Wang S, Su JH, Zhang F, Zhuang X (2016) An RNA-aptamer-based two-color CRISPR labeling system. *Sci Rep* 6:26857.
42. Oakley JL, Coleman JE (1977) Structure of a promoter for T7 RNA polymerase. *Proc Natl Acad Sci USA* 74:4266–4270.
43. Guschin DY, et al. (2010) A rapid and general assay for monitoring endogenous gene modification. *Methods Mol Biol* 649:247–256.
44. Kan Y, Ruis B, Lin S, Hendrickson EA (2014) The mechanism of gene targeting in human somatic cells. *PLoS Genet* 10:e1004251.
45. Revyakin A, Liu C, Ebright RH, Strick TR (2006) Abortive initiation and productive initiation by RNA polymerase involve DNA scrunching. *Science* 314:1139–1143.
46. Joo C, Ha T (2012) Labeling DNA (or RNA) for single-molecule FRET. *Cold Spring Harb Protoc* 2012:1005–1008.